Physics and Imaging in Radiation Oncology 16 (2020) 109–112

Contents lists available at ScienceDirect

Physics and Imaging in Radiation Oncology

journal homepage: www.sciencedirect.com/journal/physics-and-imaging-in-radiation-oncology

Technical Note

Dosimetric and geometric end-to-end accuracy of a magnetic resonance guided linear accelerator

Luisa S. Stark *, Nicolaus Andratschke, Michael Baumgartl, Marta Bogowicz, Madalyne Chamberlain, Riccardo Dal Bello, Stefanie Ehrbar, Zaira Girbau Garcia, Matthias Guckenberger, Jérôme Krayenbühl, Bertrand Pouymayou, Thomas Rudolf, Diem Vuong, Lotte Wilke, Mariangela Zamburlini, Stephanie Tanadini-Lang

University Hospital Zürich, Department of Radiation Oncology, Zurich, Switzerland

ARTICLE INFO

Keywords:
MR-Linac
Treatment adaption
Gating
End-to-end test

ABSTRACT

The introduction of real-time imaging by magnetic resonance guided linear accelerators (MR-Linacs) enabled adaptive treatments and gating on the tumor position. Different end-to-end tests monitored the accuracy of our MR-Linac during the first year of clinical operation. We report on the stability of these tests covering a static, adaptive and gating workflow. Film measurements showed gamma passing rates of 96.4% ± 3.4% for the static tests (five measurements) and for the two adaptive tests 98.9% and 99.99%, respectively (criterion 2%/2mm). The gated point dose measurements in the breathing phantom were 2.7% lower than in the static phantom.

1. Introduction

Magnetic resonance guided radiotherapy (MRgRT) potentially allows smaller margins around the target volume due to real time imaging with enhanced soft-tissue contrast [1,2]. The sparing of organs at risk may be improved while maintaining a high coverage of the tumor [3]. There is the potential to compensate inter- and intra-fractional motion by adapting the treatment plan to the actual anatomical situation [4,5] and by gating the treatment beam [6,7]. The clinical introduction of MRgRT was boosted in the last decade [8–12]. In 2017 the first patient was treated on a MR-Linac system, where an MR scanner and a linear accelerator (Linac) were combined [13]. The clinical introduction of these hybrid systems created new challenges in the quality assurance (QA) [14,15], since their overall stability is sensitive to different factors. The MR and computer tomography (CT) images need to be registered. The MR imaging isocenter must be aligned with the radiation isocenter. The electron density map is established from the CT and deformed to match the actual MR image. The dose deposition is influenced by the magnetic field, which alters the path of the charged secondary particles. The radio frequency (RF)-coils of the MR system need to be correctly positioned around the patient. MR image quality is crucial for both adaptation (image fusion) and irradiation gating (real-time cine images).

Well established QA procedures assess the single steps in the complex workflow [16], but uncertainties may accumulate over the treatment chain. New phantoms, visible on MR and CT images, were developed [14,17,18], but experience on the stability and achievable precision is still rare [19,20].

Different end-to-end tests were performed to check the complex chain of MRgRT. We report on the accuracy of the 6 MV flattening filter free (6FFF) Linac in the 0.35 T magnetic field in a static set up, for an adaptive and in a gated workflow. The results from film measurements of the 2D dose distribution and from point dose measurements are presented. The aim of this study was to show the geometric and dosimetric stability of our MR-Linac.

2. Materials and methods

During the first year of treatment at the MRIdian (Viewray, Oakwood Village, OH, USA), the 2D dose distribution and the gating performance of the machine were measured alternating every second month.

2.1. 2D dose distribution

The first five measurements of the dose distribution were performed in a spherical phantom (Lucy 3D QA phantom, Standard Imaging inc.,

* Corresponding author at: Radiation Oncology, University Hospital Zürich, Rämistrasse 100, CH-8091 Zürich, Switzerland.
E-mail address: luisasabrina.starkschneebeli@usz.ch (L.S. Stark).

https://doi.org/10.1016/j.phro.2020.09.013
Received 12 June 2020; Received in revised form 29 September 2020; Accepted 30 September 2020
Available online 8 November 2020

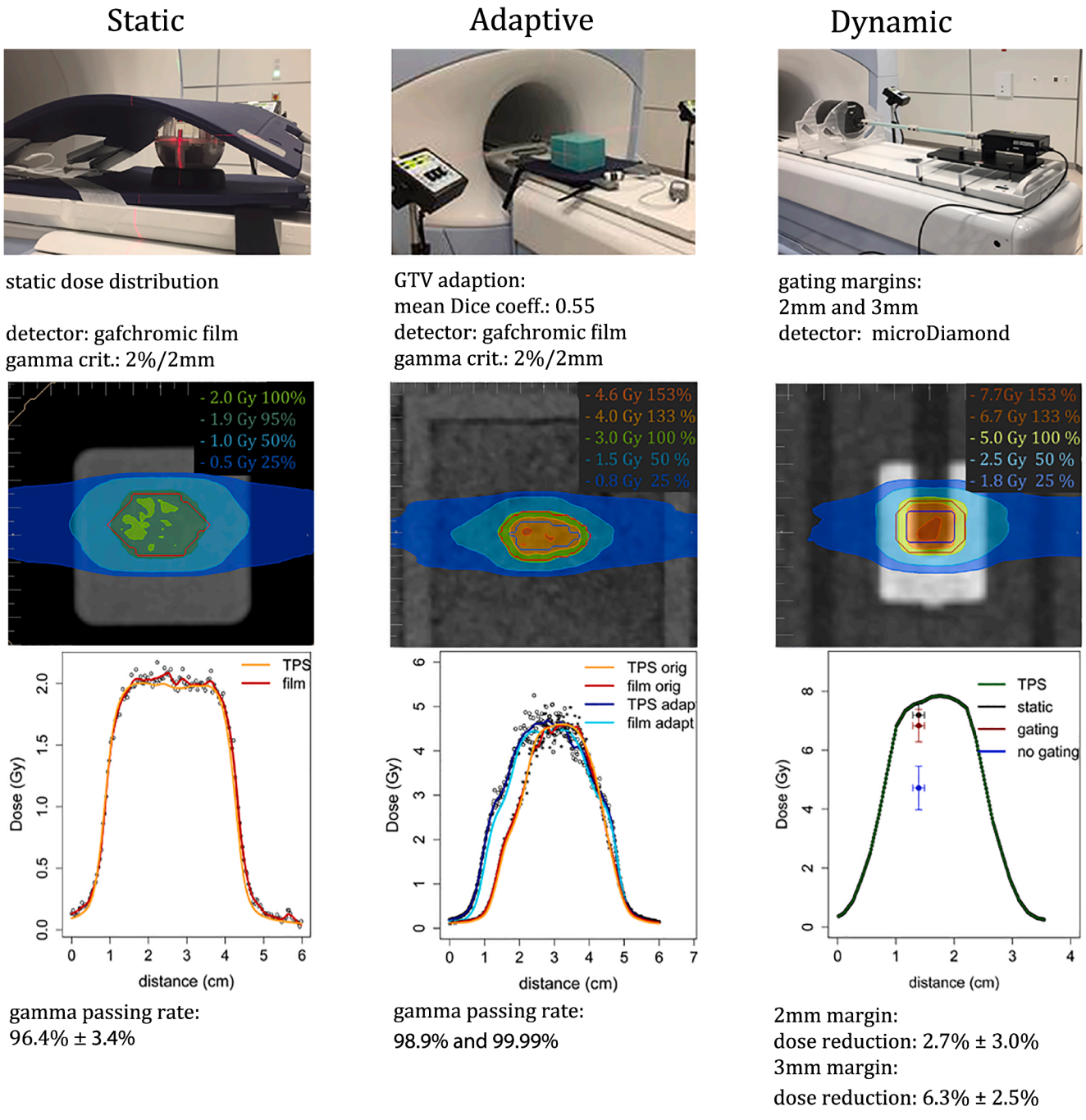

Fig. 1. Set-up for the three different end-to-end tests. On top, the phantoms are shown, first the spherical phantom followed by the in-house made silicon phantom and the thorax motion phantom. Below, the characteristics of the static, adaptive and gating measurements are indicated. In the next row the dose distribution in the TPS is displayed. Then, the longitudinal measured and planned dose profiles are shown for the static and adaptive tests. For the gating tests the calculated longitudinal dose profile is combined with the point dose measurements.

Middleton, Wisconsin, USA). An IMRT plan with 11 beams and a homogeneously prescribed dose of 2 Gy was irradiated. An MR visible insert allowed the registration of the MR images with the CT images. The plan was calculated on the MR images, taking the electron densities from the registered pretreatment CT into account. For the measurements, the spherical phantom was placed on the RF-coil and aligned to the lasers before it was moved to the treatment isocenter. An MR scan was used for fine adjustments. The dose was measured on a horizontal gafchromic EBT3 film (Ashland Global Specialty Chemicals Inc., Covington, Kentucky, USA) (Fig. 1) within the phantom. Afterwards, a film patch was irradiated under reference conditions for the absolute dose calibration. The film was analyzed 24 h later with the FilmQA software (Ashland Global Specialty Chemicals Inc., Covington, Kentucky, USA). The isocenter from the film was aligned with the isocenter of the TPS (treatment planning system) to perform a gamma analysis, applying a criterion of 2%/2 mm (dose difference with respect to the local dose/distance-to-agreement) [21]. No threshold was set on the background dose. The uncertainty was determined as the standard deviation of the measurements. After the first five measurements, we started to include the online plan adaption. To facilitate the set-up, a new cuboid silicon phantom (19 cm × 23 cm × 17 cm, silicon rubber, KauPo, Plankenhorn, Spaichingen, Germany) (Fig. 1) was developed. On the central horizontal plane a frame for a radiochromic film was integrated, allowing the precise positioning of the film. For the adaptive workflow an IMRT plan

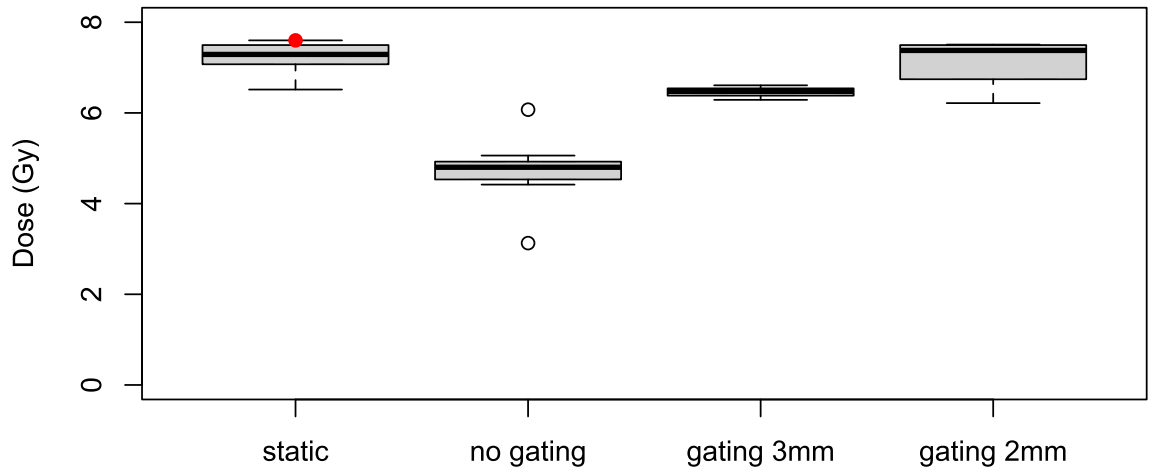

Fig. 2. Point dose measurements in the static phantom, in the breathing phantom but without gating, in the breathing phantom with a 3 mm gating window around the GTV and in the breathing phantom with a 2 mm gating window around a surrogate tracking structure. The red dot in the first column corresponds to the dose in the TPS.

with 11 beams prescribing 3 Gy to the 65% isodose line was calculated.

The silicon phantom is highly visible in the CT and the MR, which makes the deformable registration of the electron density map possible. It was placed on the RF-coil, aligned to the lasers and shifted to the isocenter, before an MR scan was performed. After matching the actual MR images with the reference, the structures of the plan were copied to the new MR scan and were adapted to simulate an anatomical change. The mean Dice coefficient [22,23] of the original gross tumor volume (GTV) and the adapted GTV was 0.55. In a next step a full adaption of the plan was performed, where the individual segments of the beams were optimized according to the changed GTV before the plan was irradiated. The original plan was irradiated as well as the plan which was adapted on the real time MR. Both dose distributions were measured and compared to the calculated doses (Fig. 1), applying a gamma evaluation criterion of 2%/2 mm.

2.2. Point dose measurements

The gating performance of the MR-Linac was evaluated in the dynamic thorax phantom (CIRS Inc., Norfolk, Virginia, USA) using a 7-field IMRT plan (Fig. 1). A dose of 5 Gy was prescribed to the 65% isodose line covering the planning target volume (PTV), simulating an SBRT (stereotactic body RT) treatment. The PTV was derived from the GTV by a margin expansion of 3 mm. Within these 3 mm the dose dropped from 6.75 Gy to 5 Gy, corresponding to a dose gradient of 0.58 Gy/mm. A microDiamond detector (PTW Freiburg, Freiburg, Germany) was inserted into a target rod moving longitudinally with an amplitude of 7.5 mm within a body-like support structure. The amplitude was defined between the midline and inhale/exhale position of the motion. As a motion pattern, a $\cos^4$ function with a period of 4 sec was applied. In a first setup, the GTV of 1.2 cm^3 was enlarged by 3 mm to define the gating window (3 measurements). In a second set- up, a surrogate tracking structure was used for gating to simulate an anatomical situation with low contrast (4 measurements). The surrogate structure, an insert in the phantom, was enlarged by 2 mm. The beam was switched on as long as more than 95% of the target was within the gating window. To study the effects of breathing, the recorded point doses were compared to the measurements in a static phantom and to the dose measured in the breathing phantom without applying gating (9 measurements each). A positioning uncertainty of 1 mm was assumed. The uncertainties in the dose were calculated as the standard deviation of the measurements. Since the microDiamond detector was aligned parallel to the magnetic field, the effect of the magnetic field on the detector could be neglected [24].

3. Results

The gamma evaluation of the five films measuring the non-adapted dose distribution in the spherical phantom showed a mean passing rate of 96.4% ± 3.4% for a 2%/2 mm criterion. The passing rates of the gamma analysis of the films could be enhanced by the use of the new cuboid silicon phantom. The evaluation of the first two adapted films showed passing rates of 98.9% and 99.99% with a criterion of 2%/2 mm.

The point dose measurements performed with simulated breathing showed a mean dose reduction of 34% ± 13% if no gating was applied compared to the measurements in a static phantom (Fig. 2). If the irradiation was gated using a gating window of 3 mm around the GTV, the measured dose was reduced by 6.3% ± 2.5%. If a surrogate tracking structure with a boundary of 2 mm was used as gating window, the dose was reduced by 2.7% ± 3.0%.

4. Discussion

The MR-Linac hybrid systems include new hardware solutions and calculation algorithms. A careful evaluation of the whole workflow is mandatory to guarantee safe treatments. In this report three different types of end-to-end tests are presented (Fig. 1).

The 2D dose distribution showed a high precision of the 6 MV FFF beam and the collimation system of the MR-Linac.

The image registration and the electron density map calculation are sensitive steps in adaptive treatments. To test the adaptive workflow an in-house made, homogeneous silicon phantom was used in order to have MRI signal across the whole phantom. In the presented work the adapted dose distribution corresponded with high precision to the calculated dose, gamma passing rates of 98.9% and 99.99% with a criterion of 2%/2 mm were achieved. In summary, the 2D dose distributions measured by radiographic films in a static phantom showed an excellent agreement with the planned dose distribution. Including all our measurements (spherical phantom and silicon cuboid) a mean gamma passing rate of 97.3% ± 3.2% was recorded. The passing rates are consistent with those reported in [19] for their MR-Linac (97.3% ± 2.3% for a criterion of 2%/2 mm). Due to the cuboid form of the phantom, the setup uncertainty could be reduced compared to the positioning error of the spherical phantom, which includes a 3D rotation, that can not be corrected by the couch of our MR-Linac.

The presented tests were performed with an arbitrary target. For future studies the phantom should include inhomogeneities that can be used both to define the target and test the registration algorithm based

upon internal structures.

The gating performance of the system was studied in the moving thorax phantom. The gating window influenced the measured dose for an inhomogeneous prescription to a small target volume (1.2 cm^3). The peaked dose distribution of a typical SBRT plan seems broadened by the breathing motion. The dose reduction depended on the size of the margin around the tracking structure. For a 3 mm margin a dose reduction of 6.3% ± 2.5% was recorded. If the gating margin was 2 mm, the dose was reduced by 2.7% ± 3% compared to the dose in a static phantom. Depending on the speed of motion and the latency of the system, the margin of the gating window, the size of the target volume and the planned dose gradient, a dose reduction has to be taken into account. In this study point dose measurements were performed in the moving phantom, but also 2D measurements of the dose distribution in the moving phantom would be interesting. [20] compared the dose distribution by film measurements for static and gated treatments on their MR-Linac. Gamma passing rates above 95% for a criterion of 4%/3 mm were reported for a gating window margin of 3 mm while allowing 10% of the target outside the gating boundary.

In conclusion, the three different types of end-to-end tests demonstrated a high geometric and dosimetric accuracy of our MR-Linac throughout the first year of treatment, which allows for precise stereotactic body treatments, accurate gating for moving targets and reliable adaption of the treatment plan.

Declaration of Competing Interest

The authors declare that they have no known competing financial interests or personal relationships that could have appeared to influence the work reported in this paper.

Acknowledgements

This paper is part of a special issue that contains contributions originally submitted to the scientific meeting MR in RT, which was planned to take place 05/2020, organized by the German Research Center (DKFZ) in Heidelberg. We acknowledge funding by DKFZ for the publication costs of this special issue.

References

[1] Paganelli C, Whelan B, Peroni M, Summers P, Fast M, Van de Lindt T, et al. MRI-guidance for Motion Management in External Beam Radiotherapy: Current Status and Future Challenges. Phys Med Biol 2018;63:22TR03. https://doi.org/10.1088/1361-6560/aaebcf.

[2] Klüter S. Technical design and concept of a 0.35 T MR-Linac. Clin Transl Radiat Oncol 2019;18:98–101. https://doi.org/10.1016/j.ctro.2019.04.007.

[3] Kron T. Reduction of margins in external beam radiotherapy. J Med Phys 2008;33 (2):41. https://doi.org/10.4103/0971-6203.41190.

[4] Bohoudi O, Bruynzeel AME, Senan S, Cuijpers JP, Slotman BJ, Lagerwaard FJ, Palacios MA. Fast and robust online adaptive planning in stereotactic MR-guided adaptive radiation therapy (SMART) for pancreatic cancer. Radiother Oncol 2017; 125(3):439–44. https://doi.org/10.1016/j.radonc.2017.07.028.

[5] Hunt A, Hansen VN, Oelfke U, Nill S, Hafeez S. Adaptive Radiotherapy Enabled by MRI Guidance. Clin Oncol 2018;30(11):711–9. https://doi.org/10.1016/j.clon.2018.08.001.

[6] Yan Di, Vicini F, Wong J, Martinez A. Adaptive radiation therapy. Phys Med Biol 1997;42(1):123–32. https://doi.org/10.1088/0031-9155/42/1/008.

[7] Lagendijk JJW, Raaymakers BW, Raaijmakers AJE, Overweg J, Brown KJ, Kerkhof EM, van der Put RW, Hårdemark B, van Vulpen M, van der Heide UA. MRI/linac integration. Radiother Oncol 2008;86(1):25–9. https://doi.org/10.1016/j.radonc.2007.10.034.

[8] Fallone BG. The Rotating Biplanar Linac–Magnetic Resonance Imaging System. Semin Radiat Oncol 2014;24(3):200–2. https://doi.org/10.1016/j.semradonc.2014.02.011.

[9] Jaffray DA, Carlone MC, Milosevic MF, Breen SL, Stanescu T, Rink A, Alasti H, Simeonov A, Sweitzer MC, Winter JD. A facility for magnetic resonance–guided radiation therapy. Semin Radiat Oncol 2014;24(3):193–5. https://doi.org/10.1016/j.semradonc.2014.02.012.

[10] Keall PJ, Barton M, Crozier S. The australian magnetic resonance imaging–linac program. Semin Radiat Oncol 2014;24(3):203–6. https://doi.org/10.1016/j.semradonc.2014.02.015.

[11] Lagendijk JJW, Raaymakers BW, Van den Berg CAT, Moerland MA, Philippens ME, van Vulpen M. MR guidance in radiotherapy. Phys Med Biol 2014;59(21):R349–69. https://doi.org/10.1088/0031-9155/59/21/R349.

[12] Mutic S, Dempsey JF. The viewray system: magnetic resonance–guided and controlled radiotherapy. Semin Radiat Oncol 2014;24(3):196–9. https://doi.org/10.1016/j.semradonc.2014.02.008.

[13] Raaymakers B, Jürgenliemk-Schulz I, Bol G, Glitzner M, Kotte A, Van Asselen B, et al. First patients treated with a 1.5 T MRI-Linac: clinical proof of concept of a high-precision, high-field MRI guided radiotherapy treatment. Phys Med Biol 2017; 62:L41–50. https://doi.org/10.1088/1361-6560/aa9517.

[14] Elter A. End-to-end test of an online adaptive treatment procedure in MR-guided radiotherapy using a phantom with anthropomorphic structures. Phys Med Bio 2019;64:225003. https://doi.org/10.1088/1361-6560/ab4d8e.

[15] Pasler M, Hernandez V, Jornet N, Clark CH. Novel methodologies for dosimetry audits: Adapting to advanced radiotherapy techniques. Phys Imag Radiat Oncol 2018;5:76–84. https://doi.org/10.1016/j.phro.2018.03.002.

[16] Tetar SU, Bruynzeel AME, Lagerwaard FJ, Slotman BJ, Bohoudi O, Palacios MA. Clinical implementation of magnetic resonance imaging guided adaptive radiotherapy for localized prostate cancer. Phys Imag Radiat Oncol 2019;9:69–76. https://doi.org/10.1016/j.phro.2019.02.002.

[17] Niebuhr NI, Johnen W, Güldaglar T, Runz A, Echner G, Mann P, Möhler C, Pfaffenberger A, Jäkel O, Greilich S. Technical Note: Radiological properties of tissue surrogates used in a multimodality deformable pelvic phantom for MR-guided radiotherapy: Tissue surrogates for a multimodality phantom. Med Phys 2016;43(2):908–16. https://doi.org/10.1118/1.4939874.

[18] Pappas E, Kalaitzakis G, Boursianis T, Zoros E, Zourari K, Pappas EP, et al. Phys Med Biol 2019;64:225009.

[19] Gungor G, Korkmaz L, Kayalilar N, Gokhan A, Bulent Y, Teuta Z, et al. Multichannel Film Dosimetry for Quality Assurance of Intensity Modulated Radiotherapy Treatment Plans Under 0.35 T Magnetic Field. Cureus 2020;12: e7334. https://doi.org/10.7759/cureus.7334.

[20] Lamb JM, Ginn JS, O'Connell DP, Agazaryan N, Cao M, Thomas DH, Yang Y, Lazea M, Lee P, Low DA. Dosimetric validation of a magnetic resonance image gated radiotherapy system using a motion phantom and radiochromic film. J Appl Clin Med Phys 2017;18(3):163–9. https://doi.org/10.1002/acm2.12088.

[21] Low DA, Harms WB, Mutic S, Purdy JA. A technique for the quantitative evaluation of dose distributions. Med Phys 1998;25(5):656–61. https://doi.org/10.1118/1.598248.

[22] Dice LR. Measures of the Amount of Ecological Association Between Species. Ecology 1945;26:297–302. https://doi.org/10.2307/1932409.

[23] Sørensen T. A method of establishing groups of equal amplitude in plant sociology based on similarity of species and its application to analyses of the vegetation on Danish commons. Kongelige Danske Videnskabernes Selskab 1948;5:1–34.

[24] Reynolds M, Fallone BG, Rathee S. Dose response of selected solid state detectors in applied homogeneous transverse and longitudinal magnetic fields: Solid state detector dose response in magnetic fields. Med Phys 2014;41(9):092103. https://doi.org/10.1118/1.4893276.